Theoretical analysis of nonlinear pulse propagation in ferrite-dielectric-metal structures based on the nonlinear Schrödinger equation with higher order terms

Alexander S. Kindyak,[a] Mark M. Scott,[b] and Carl E. Patton
Department of Physics, Colorado State University, Fort Collins, Colorado 80523-1875

(Received 19 November 2002; accepted 20 January 2003)

An analysis of nonlinear magnetostatic surface wave pulse propagation in planar ferrite-dielectric-metal (FDM) structures has been performed. The analysis was based on numerical solutions to the higher-order nonlinear Schrödinger (HONLS) equation, with third-order (D_3) and nonlinear (Q) dispersion terms taken into account. The analysis focuses on (1) the crossover dispersion region for FDM structures and the point in wave-number k where the second-order dispersion parameter D_2 is a positive maximum, the Lighthill criterion for envelope soliton propagation is satisfied, and D_3 is close to zero, and (2) the end points of this crossover region where D_2 is zero. All operational HONLS equation parameters were evaluated from analytical dispersion expressions for the FDM structure and for magnetic field and structure parameters which match experiments. For (1), the pulse results indicate nondispersive propagation consistent with envelope solitons. The only effect of the Q term is to decrease slightly the propagation speed. For (2), both end points give nondispersive propagation as well. At the low-k crossover point, this result is consistent with condition $D_3Q<0$ and the existence of an analytic soliton solution. For the high-k crossover point, the nondispersive propagation is likely due simply to the relatively small value of the third-order dispersion D_3 parameter. In both cases, one finds a rapidly oscillating wave-packet structure which propagates ahead of the main pulse. For the low-k crossover point, this structure travels at approximately twice the main pulse velocity. For the high-k crossover point, the structure travels with the main pulse. The Q term has a small effect on the pulse amplitude for the low-k crossover point, and serves to reduce the pulse amplitude by 20%–30% at the high-k crossover point. PACS numbers: © *2003 American Institute of Physics.* [DOI: 10.1063/1.1559938]

I. INTRODUCTION

Due to their low-microwave loss, single-crystal yttrium iron garnet (YIG) films provide an ideal medium for research on microwave magnetic envelope (MME) solitons formed from magnetostatic wave (MSW) pulses. See, for example, Refs. 1–7. The theoretical modeling of MME solitons can be done in terms of the nonlinear Schrödinger (NLS) equation as in the above references. As shown in Ref. 8, such modeling yields a good match to the data under three conditions. First, the power levels must not be too high. Second, proper attention must be given to filtering effects due to the limited MSW passband. Third, accurate values for the NLS equation parameters, especially the dispersion coefficient, which correspond to the experiment must be used.

The NLS equation model is not adequate to model all observed MME soliton properties. The model fails, for example, if the power levels extend into the regime for higher-order solitons with more than one peak in the pulse envelope profile.[8] Furthermore, the usual NLS equation with the second-order dispersion term and the single nonlinear term cannot explain the observed power dependent soliton velocity data from Ref. 3. Zaspel *et al.*[9] were able to model these velocity effects through the inclusion of higher-order dispersion and nonlinear terms in the NLS equation. Variants of the NLS equation with these and certain other higher-order terms are sometimes referred to as the higher-order NLS, or HONLS, equation. Various HONLS equation variants have been used to model optical bright[10–12] and dark[13,14] envelope solitons. The NLS equation with a single additional term for third-order dispersion has been used to model nonlinear magnetostatic forward volume wave pulses in single films.[15,16]

This work presents the modeling of nonlinear MME pulse propagation in ferrite-dielectric-metal (FDM) structures in the magnetostatic surface wave (MSSW) configuration based on the NLS equation with higher-order dispersion and nonlinear response terms taken into account. The combination of the MSSW configuration, the FDM structure, and a consideration of the NLS analysis with higher-order terms presents a unique situation for the study of the effect of higher-order terms, the nonlinear MME pulse response, and soliton or solitonlike propagation characteristics.

In isolated films or slabs, the MSSW propagation configuration does not support bright soliton formation. The second-order dispersion coefficient parameter $D_2 = \partial^2 \omega_k / \partial k^2$, where ω_k denotes the spin wave frequency and

[a]On leave from the Minsk Research Institute of Radiomaterials, Kizhevatova St. 86, 220024, Minsk, Belarus.
[b]Electronic mail: mscott@lamar.colostate.edu

 © 2003 American Institute of Physics

Downloaded 03 Jul 2003 to 129.82.31.230. Redistribution subject to AIP license or copyright, see http://ojps.aip.org/japo/japcr.jsp

k is the wave number, is negative for MSSW signals. The lowest-order nonlinear response coefficient $N=\partial\omega_k/\partial|u|^2$, where u is a complex scalar amplitude which scales with the dynamic magnetization **m**, is also negative. The usual condition for soliton formation in nonlinear dispersive media is that the D_2N product is negative and this condition is not satisfied.

In FDM structures, however, the ferrite-dielectric-metal sandwich geometry modifies the ω_k versus k dispersion curve in such a way as to produce a region in k and in frequency where D_2 changes from negative to positive. See De Wames and Wolfram[17] and Bongianni.[18] Boardman and Nikitov[19] pointed out that this inversion also leads to the possibility of MME solitons formed from MSSW pulses. Nikitov *et al.*[20] reported modulational instability data which were consistent with this possibility. Uehara *et al.*[21] modeled the MME pulse propagation in such structures based on the NLS equation. These authors also included the effect of a third-order dispersion term on the MME pulse response and found that this higher-order term serves to modify the solitonlike response.

The purpose of this work was to extend the analysis of nonlinear MSSW pulses propagation for FDM structures initiated in Refs. 21 and 22 in several ways, all based on the consequences of the $D_2>0$ crossover region discussed above. First, at the crossover points, one has D_2 equal to zero and the effects of the third-order dispersion $D_3=\partial^3\omega_k/\partial k^3$ on the nonlinear pulse response may be examined in detail. Second, it turns out that D_3 has *opposite signs* at the $D_2=0$ crossover points. Third, it also turns out that D_3 has a *zero crossing* close to the point where D_2 has its positive maximum. The first two considerations makes it possible to use the $D_2=0$ crossover points to examine the effect of positive and negative values of the third-order dispersion on the pulse response. This sign change is particularly interesting because the nonlinear dispersion term in the HONLS equation, $Q=\partial N/\partial k$, is negative over the entire crossover range. At the low-k crossover point, the validity of the condition $QD_3<0$ leads to analytic soliton solutions. This condition is not satisfied at the high-k crossover point. The third consideration, with $D_3=0$, provides the opportunity to study the effect of the k-dependent nonlinear response HONLS equation term $Q=\partial N/\partial k$ on the nonlinear pulse response.

The nonlinear pulse propagation analysis was based on numerical solutions to the HONLS equation with the terms indicated above included in the modeling. The analysis yielded several results. First, for k at the maximum D_2 point in the middle of the crossover region, the numerical data confirm the nondispersive solitonlike pulse propagation expected from the Lighthill criterion. The inclusion of a nonzero Q leads only to a small reduction in the pulse velocity. In the case of optical solitons, in contrast, the Q term has been reported to produce a pronounced pulse asymmetry.

Second, it is found that the $D_2=0$ crossover points at high and low k give quite different pulse propagation characteristics. At the low-k crossover point, where D_3 is positive and relatively large, the propagation is nondispersive and solitonlike. The soliton is accompanied by a radiative wave packet, much like in the optical case. This soliton like propagation is consistent with the existence of an analytic soliton solution at this low-k crossover point due to the $QD_3<0$ condition at this point. At the high-k crossover point, where D_3 is negative and relatively small, the numerical simulations give quasi-stable pulse propagation with low dispersion. Here, there is a significant radiative tail. It is noteworthy that the high-k crossover point gives quasi-stable propagation even though the soliton condition $QD_3<0$ is not satisfied. This is likely due to the small dispersion.

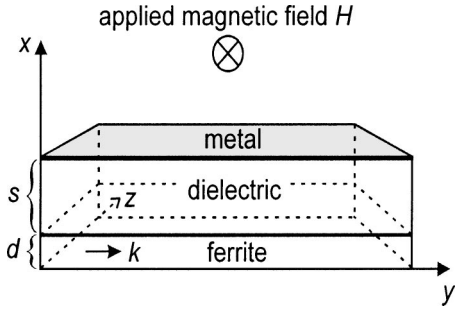

FIG. 1. Schematic diagram of ferrite-dielectric-metal (FDM) structure used for the analysis. The ferrite layer of thickness d is separated from the thin metal layer by a dielectric layer of thickness s. Pulse propagation is taken to be in the $+y$ direction and defined by a carrier wave-number k, as indicated. The in-plane applied magnetic-field H is perpendicular to the pulse propagation direction and along $+z$. All layers are taken to be unbounded in the y and z directions.

Section II presents details on the FDM structure, the dispersion analysis, the HONLS equation formalism and numerical solutions, and operating point considerations for the crossover wave-number regime. Section III presents numerical results on nonlinear pulse propagation at the $D_3=0$ point in the middle of the crossover regime and at the $D_2=0$ crossover points which define the soliton k region. The equations for the analytic dispersion solution for the FDM structure are given in the appendix.

II. MODEL AND ANALYSIS

Figure 1 shows the geometry of the FDM structure which was used for the dispersion analysis and the numerical evaluations. The ferrite film or slab of thickness d is positioned in the $y-z$ plane with the propagation direction and wave-vector **k** along $+y$ and the applied static magnetic-field **H** along $+z$. The dielectric layer of thickness s is positioned above the ferrite layer and is capped with an infinitesimally thin metal layer. All layers are taken to be infinite and isotropic in the y and z directions. For simplicity, the dielectric layer is taken to have a relative dielectric constant of unity, the same as vacuum. Propagation is taken to be one dimensional, with no variation in the dynamic response with z. In the $s\gg 2\pi/k$ limit, the geometry of Fig. 1 reduces to the usual Damon–Eshbach MSSW configuration for an isolated ferrite film.

For the FDM structure in Fig. 1, one can obtain the linear dispersion relation $\omega_k=f(k, M_s)$ for the guided wave propagation in the y direction in analytic form.[22] For convenience in the extension of the analysis to the nonlinear case,

Downloaded 03 Jul 2003 to 129.82.31.230. Redistribution subject to AIP license or copyright, see http://ojps.aip.org/japo/japcr.jsp

the magnetization of the ferrite, denoted as M_s, is included specifically as a control parameter. The analytical dispersion relation may be written in the form

$$\omega_k=\frac{1}{4}\omega_M\alpha_k(1-\beta_k) + \sqrt{\left[\frac{1}{2}(\omega_M+2\omega_H)+\frac{1}{4}\omega_M\alpha_k(1-\beta_k)\right]^2-\frac{1}{4}\omega_M^2\beta_k}. \tag{1}$$

In Eq. (1), $\omega_M=|\gamma|4\pi M_s$ and $\omega_H=|\gamma|H$ express the magnetization and applied magnetic field, respectively, in frequency units. The α_k and β_k correspond to exponential k functions given by $\alpha_k=e^{-2ks}$ and $\beta_k=e^{-2kd}$, respectively. The γ parameter in ω_M and ω_H is the electron gyromagnetic ratio. Note that the equations in Ref. 22 which correspond to Eq. (1) above contain type setting errors.

Now consider the HONLS equation model which is used for the pulse propagation analysis. The needed variant of the HONLS equation for the propagation of an envelope function $u(y,t)$ may be written in the form

$$i\left[\frac{\partial u}{\partial t}+v_g\frac{\partial u}{\partial y}\right]+\frac{1}{2}D_2\frac{\partial^2 u}{\partial y^2}-N|u|^2u - i\left[\frac{D_3}{6}\frac{\partial^3 u}{\partial y^3}-Q\frac{\partial(|u|^2u)}{\partial y}\right]=0. \tag{2}$$

Equation (2) may be obtained through the usual method of envelopes expansion and operator substitution, with terms extended to include the higher-order D_3 and Q terms defined in the introduction. These higher-order terms are shown in the second square bracket. Without these terms, Eq. (2) constitutes the usual NLS equation considered in Ref. 4, for example. The v_g parameter in Eq. (2) is the wave-packet group velocity in the wide packet low-power limit defined by $v_g=\partial\omega_k/\partial k$. All derivatives are evaluated in the $u=0$ limit and at the desired operating point k and ω_k values. Note that the Q term corresponds to the dependence of the group velocity on the wave power amplitude $|u|^2$. Note also that there is an analytical soliton solution to Eq. (2) when the condition $QD_3<0$ is satisfied, in contrast to the soliton solution condition $ND_2<0$ which holds for the NLS equation. See Ref. 9, for example.

The v_g, D_2, and D_3 coefficients in Eq. (2) may be evaluated directly from Eq. (1). The N and Q coefficients may also be obtained from Eq. (1). This is done in three steps. The ω_M parameter in Eq. (1) is first replaced by

$$\tilde{\omega}_M=|\gamma|4\pi M_s(1-|u|^2). \tag{3}$$

One then proceeds to evaluate the appropriate derivatives. Last, one sets u to zero and obtains the N and Q expressions needed for the analysis. Analytic expressions for all of the HONLS equation coefficients in Eq. (2) are tabulated in the appendix.

As noted in the introduction, the FDM structure leads to characteristic variations in the D_2 and D_3 parameters which make possible a systematic examination of the effect of the D_3 and Q terms on the nonlinear pulse propagation. Figure 2 shows the key variations which are of interest here, namely, the crossover behavior of the second- and third-order dispersion coefficients D_2 and D_3 as a function of the wave-number k. For the evaluations shown, the field H was set to 1.0 kOe, and $4\pi M_s$ and $|\gamma|$ were set at the YIG values of 1750 G and 1.76×10^7 rad/Oe·s, respectively. The FDM structure d and s spacing values were set at 0.028 and 0.254 mm, respectively. These values correspond to those used in MSSW modulation instability experiments on single layer YIG films.[20]

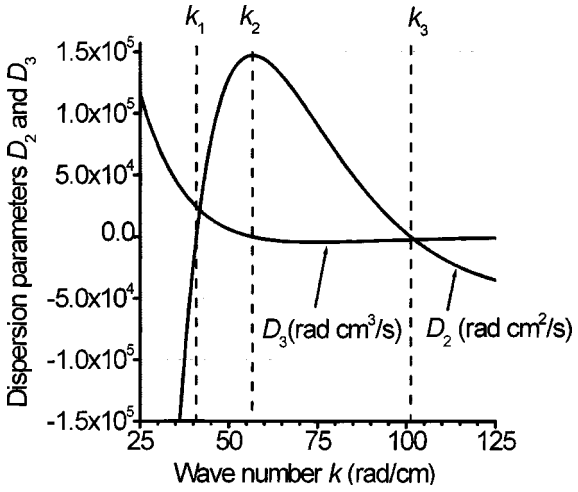

FIG. 2. Second- and third-order MSSW dispersion coefficients D_2 and D_3, respectively, as a function of wave-number k. The curve labeled D_2 indicates the second-order dispersion in cm^2/s. The curve labeled D_3 indicates the third-order dispersion in cm^3/s. The vertical lines labeled k_1, k_2, and k_3 indicate the values of the wave number which will be considered in the simulations.

The curves in Fig. 2 show that D_2 changes from negative to positive for a range of k values from about 40 to 100 rad/cm. Within this range, D_2 shows a positive maximum and D_3 changes from large and positive to small and negative for a k value close to 55 rad/cm. The vertical dashed lines at the D_2 crossover points designate the corresponding k values, labeled k_1 and k_3 at the top of the graph. The dashed vertical line at $k=k_2$ designates the D_3 crossover point.

Table I lists the k and ω_k operating points, and the HONLS equation parameters for the k_1, k_2, and k_3 operating point positions indicated above. Note that while the Lighthill criterion $ND_2<0$ is satisfied over the entire crossover range $k_1<k<k_3$, the HONLS condition for analytic soliton solutions $QD_3<0$ is only satisfied for $k_1<k<k_2$. This is because Q is negative over the entire crossover range. The three operating points in the table will be used for the pulse propagation results given below.

It is useful to reiterate the characteristics of the dispersion and nonlinear parameters which make these points of special interest. First, it has been made clear above and elsewhere that the second-order dispersion parameter D_2 changes from negative to positive over the entire range $k_1<k<k_3$ and offers the possibility of soliton formation and propagation. Such effects have been studied in Refs. 21 and 22. Second, the $D_2=0$ crossover points at k_1 and k_3 allow

Downloaded 03 Jul 2003 to 129.82.31.230. Redistribution subject to AIP license or copyright, see http://ojps.aip.org/japo/japcr.jsp

TABLE I. List of parameters used for the nonlinear pulse propagation HONLS equation numerical simulations at the operating wave-number points k_1, k_2, and k_3 indicated in Fig. 2. The symbolic headers give the MSSW carrier frequency $\omega_k/2\pi$ and wave-number k, the wave-packet group-velocity v_g, the group-velocity dispersion D_2, the third-order dispersion D_3, the nonlinear coefficient N, and the nonlinear dispersion parameter Q. Detailed setup conditions and definitions of these parameters are given in Sec. II

Points	$\omega_k/2\pi$ (MHz)	k (rad/cm)	v_g (cm/s)	D_2 (rad cm^2/s)	D_3 (rad cm^3/s)	N (rad/s)	Q (cm/s)
k_1	4839.0	40.82	5.44×10^6	0	$+2.43\times10^4$	-1.10×10^{10}	-1.59×10^7
k_2	4853.0	56.65	7.09×10^6	1.464×10^5	0	-1.13×10^{10}	-1.66×10^7
k_3	4921.0	101.2	1.04×10^7	0	-2.312×10^3	-1.21×10^{10}	-1.77×10^7

one to examine the effects of only the third-order dispersion coefficient D_3 on the nonlinear pulse propagation. The fact that D_3 has a zero crossing in the middle of the crossover regime, is large and positive at k_1, and is small and negative at k_3 makes these crossover points of even greater interest. Finally, the zero value of D_3 at point k_2 makes it possible to examine the effect of the higher-order nonlinear Q term on the pulse response in the absence of higher-order dispersion effects. Numerical pulse propagation results for these three situations will be considered in Sec. III.

The numerical results in the next section address these issues. First, the pulse propagation response will be examined at the $k=k_2$ operating point. With D_3 equal to zero at this point, the analysis with Q also equal to zero corresponds to the standard NLS equation situation. The Q term inclusion can then elucidate the effect of this nonlinear term on the response. Second, the k_1 and k_3 end points will be considered. Here one can examine the effect of the very different D_3 values on the pulse propagation. This is done for $Q=0$. Finally, point k_3 is further examined with Q set to the correct value.

The numerical analysis was done for an initial spatial pulse in the form of a super Gaussian

$$u(y,0)=u_0e^{-(y/2\Delta)^4}, \tag{4}$$

where u_0 denotes the initial envelope amplitude and Δ is a width parameter for the pulse. Equation (2), with appropriate numerical values for the parameters listed in Table I, was then solved by the split-step method.[23] This method allows one to obtain the spatial dependence of the pulse intensity over a range of specified times. Form these data the time dependence of the pulse intensity may be reconstructed at a specified point in space.

III. RESULTS

Figure 3 shows representative $|u|^2$ versus time profiles for an operating point at $k=k_2$, the point for which D_3 is zero and D_2 is a positive maximum. Profiles are shown for a sequence of increasing y values, as indicated. The solid curves show profiles obtained for $Q=0$ in the standard NLS equation limit with no higher-order terms. The dashed curves show the computed profiles for the applicable $k=k_2$ operating point Q value of -1.66×10^7 cm/s. The initial spatial pulse was configured with an amplitude $u_0=0.09$ and width parameter $\Delta=0.0709$ cm. This Δ corresponds to an input microwave pulse width of about 10 ns. The amplitude u_0 for the numerical calculations to follow was chosen as the lowest value u_0 which gave quasi-stable single pulse propagation. For the calculations to follow, the values of u_0 ranged from 0.06 - 0.2. These u_0 values correspond to a dynamic magnetization $|\mathbf{m}|$ which is between 3% and 9% of M_s. These conditions match those which produce solitons in typical experiments.

First consider the solid line profiles for the NLS equation limit and $Q=0$. The simulations give a propagating pulse without dispersion spreading. Although it is not readily discernable from the pulses shown, there is an evolution from the super Gaussian input pulse shape to the expected hyperbolic secant shape for solitons as the propagation proceeds. Recall that for $k=k_2$, one has $ND_2<0$ and a corresponding analytic order one soliton solution to Eq. (2) with D_3 and Q set to zero. The solid line profiles in Fig. 3 for $y=1.0$ cm and $y=1.5$ cm closely match this analytic form.

These profiles demonstrate the soliton character of the propagation for $k=k_2$. They reconfirm the result from Ref. 21 that FDM structures can support soliton propagation in the crossover region where the second-order dispersion parameter D_2 is positive. As shown by the dashed curves in Fig. 4, the inclusion of a nonzero Q has little effect on the pulse response. These dashed line profiles indicate a slightly larger pulse velocity than for $Q=0$. There is no change in the pulse shape.

Turn now to the crossover region k_1 and k_3 end points with $D_2=0$. Figure 4 gives representative $|u|^2$ versus time profiles for $k=k_1$. The operating point parameters from Table I apply, except that the solid curves were obtained for

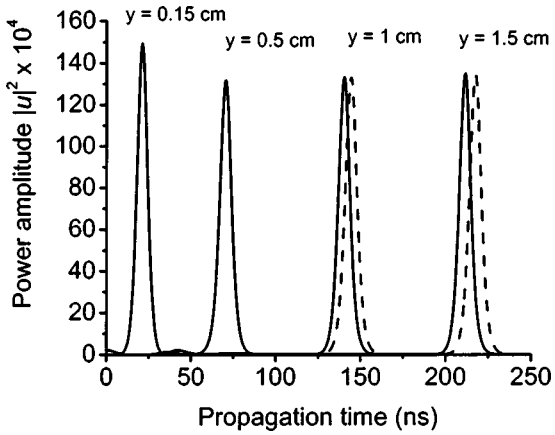

FIG. 3. Pulse profiles from the numerical simulations for wave-number point $k=k_2$ in Table I and an initial spatial pulse. The time profiles were constructed at the y-propagation distances of 0.15, 0.5, 1.0, and 1.5 cm, as indicated. The solid curves are for $Q=0$. The dashed curves are for the appropriate Q value for $k=k_2$.

Downloaded 03 Jul 2003 to 129.82.31.230. Redistribution subject to AIP license or copyright, see http://ojps.aip.org/japo/japcr.jsp

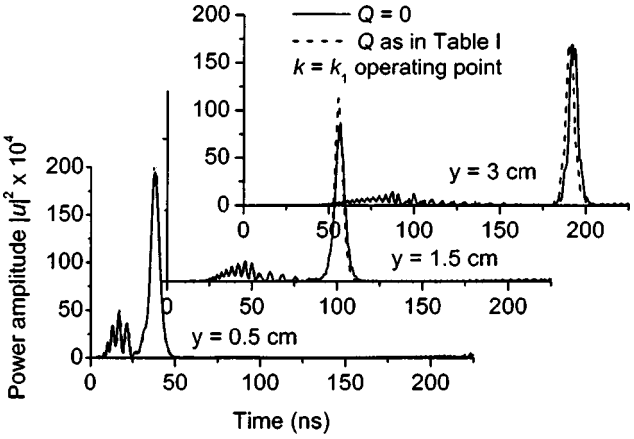

FIG. 4. Pulse profiles from the numerical simulations for wave-number point $k=k_1$ in Table I and an initial spatial pulse as indicated. The time profiles were constructed at the y-propagation distances of 0.5, 1.5, and 3.0 cm, as indicated. The solid curves are for $Q=0$. The dashed curves are for the appropriate Q value for $k=k_1$.

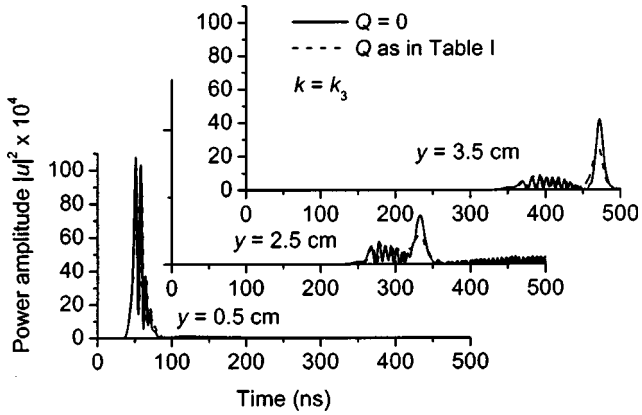

FIG. 5. Pulse profiles from the numerical simulations for wave-number point $k=k_3$ in Table I and an initial spatial pulse. The time profiles were constructed at the y-propagation distances of 0.5, 2.5, and 3.5 cm, as indicated. The solid curves are for $Q=0$. The dashed curves are for the appropriate Q value for $k=k_3$.

$Q=0$. Keep in mind that for $k=k_1$ the third-order dispersion parameter D_3 is positive and large. In addition, the condition for an analytical soliton solution to Eq. (1), $QD_3<0$, is satisfied. The dashed curves show the pulse results obtained for the applicable nonzero Q value from Table I. For all of the calculations, the $u(y,t)$ starting pulse was configured with $u_0=0.2$ and $\Delta=0.0544$ cm. This u_0 corresponds to a dynamic magnetization $|\mathbf{m}|$, which is about 9% of M_s, a factor of three larger than used for the Fig. 3 results. The Δ value corresponds to a starting pulse width of about 10 ns, the same as for the Fig. 3 profiles. It was found that if u_0 is smaller than 0.2, the pulse cannot propagate in quasi-stable form.

The data in Fig. 4 show the main features of the pulse propagation response for $k=k_1$. The main part of the pulse takes on a solitonlike nondispersive shape at long propagation distances. The inclusion of a nonzero Q has a small effect on the amplitude and velocity of the pulse, but does not affect the main characteristics of the propagation. Note that the quasi-stable propagation characteristic obtained here is consistent with the analytic soliton condition $QD_3<0$ which is valid for the $k=k_1$ operating point.

The simulations also show that a rapidly oscillating wave packet is generated. This relatively wide packet appears before the passage of the pulse. The speed of this packet is about twice the pulse velocity. At $y=1.5$ cm, this packet is well separated from the main pulse. Similar rapidly oscillating packets are found in numerical simulations based on Eq. (1) for the case of optical fibers.[11]

Figure 5 shows parallel numerical pulse evaluations for the operating point at $k=k_3$. The format is the same as for Fig. 4. The operating point parameters from Table I apply, except that the solid curves were obtained for $Q=0$. The dashed curves show the pulse results obtained for the applicable nonzero Q value from Table I. Keep in mind that for $k=k_3$ the third-order dispersion parameter D_3 is negative and about an order of magnitude smaller than for the $k=k_1$ operating point considered above. The condition for an analytical soliton solution to Eq. (1), $QD_3<0$, is not satisfied.

For all of the calculations, the $u(y,t)$ starting pulse was configured with $u_0=0.08$ and $\Delta=0.0544$ cm. This u_0 corresponds to a dynamic magnetization $|\mathbf{m}|$ which is about 3% of M_s, about the same as for the Fig. 3 calculations and substantially smaller than for Fig. 4. This Δ value corresponds to a starting pulse width of about 10 ns, the same as for Figs. 3 and 4.

The data in Fig. 5 demonstrate the pulse response for $k=k_3$. As for $k=k_1$, the main part of the pulse takes on a quasi-stable character after some propagation time and distance has elapsed. This appears to be true in spite of the fact that the analytic soliton condition $QD_3<0$ is not satisfied. One can likely attribute the quasi-stable response to the very small third-order dispersion at $k=k_3$.

The inclusion of a nonzero Q has a significant effect on the pulse at $k=k_3$ when compared to the pulse response at $k=k_1$. Here, the nonzero Q results in a decrease in the pulse power amplitude by about 30%, relative to the response for $Q=0$, for long propagation times. The nonzero Q appears to have no effect on the pulse velocity. The rapidly oscillating part of the response is also different from the situation at $k=k_1$. For $k=k_3$, this oscillating wave packet follows the main pulse at about the same velocity. The packet does not move ahead of the main pulse in time as in Fig. 4.

IV. SUMMARY AND CONCLUSION

Investigations of the influence of higher-order NLS equation terms on MSSW pulse propagation in FDM structures have been performed. In particular, the analysis focuses (1) on the crossover region in dispersion for which the Lighthill criterion for soliton propagation, $ND_2<0$, is satisfied, and (2) on the end points for this crossover region where the second-order dispersion parameter D_2 is zero. At the low-k crossover point, the HONLS equation condition for an analytic soliton solution, $QD_3<0$, is satisfied. At the high-k crossover point, this condition is not satisfied. All HONLS equation parameters for the different operating points were obtained from analytical dispersion expressions for the FDM structure under typical MSW experimental conditions.

Downloaded 03 Jul 2003 to 129.82.31.230. Redistribution subject to AIP license or copyright, see http://ojps.aip.org/japo/japcr.jsp

The results are twofold. First, they show that, in the k range where D_2 is a positive maximum, the pulse propagation is nondispersive, as expected in the regime where the Lighthill criterion is satisfied. This point in k also corresponds to a zero crossing in the third-order dispersion parameter D_3, which makes it possible to examine the effect of the nonlinear dispersion Q term on the pulse response. The numerical data show that a nonzero Q term has little effect on the pulse propagation, except for a small decrease in the pulse velocity.

The second result concerns the end points in k for the positive D_2 region. At the low k end point, where the $QD_3 < 0$ HONLS equation condition for an analytical soliton solution is valid, one finds nondispersive solitonlike propagation. This is true in spite of the rather large value of the third-order dispersion D_3 parameter. Here too, there is no major effect of a nonzero Q on the propagation properties. The only Q effect is a small change in amplitude. At the high-k end point, where the $QD_3 < 0$ HONLS equation condition for an analytical soliton solution is not valid, one also finds nondispersive solitonlike propagation. This is tentatively attributed to the relatively small value of the D_3 parameter at this k point. Both end points yield an additional rapidly oscillating envelope signal, which precedes the main pulse. At the low-k crossover point, this signal travels roughly twice as fast as the main pulse. At the high-k crossover point, this signal travels just ahead of the main pulse.

ACKNOWLEDGMENTS

This work was partly supported by the National Science Foundation, Grant No. DMR-9801649 and International Supplement DMR - 9941124. Professor A. D. Boardman, Salford University, and Dr. S. A. Nikitov, Institute of Radio Technology and Electronics, Russian Academy of Sciences, Moscow, are acknowledged for helpful discussions.

APPENDIX

The analytic expressions obtained from the dispersion relation of Eq. (1) and the recipe in Sec. II for the group velocity v_g, the dispersion parameters D_2 and D_3, and the nonlinear response parameters N and Q are given below.

For the group velocity v_g, one obtains

$$v_g = -\frac{\omega_M}{2}\left(A_k\alpha_k + \frac{T_k}{\sqrt{S_k^2 - 4\omega_M^2\beta_k}}\right), \tag{A1}$$

where the A_k, S_k, and T_k are given by

$$A_k = s - \beta_k(s+d), \tag{A2}$$

$$S_k = 2(\omega_M + 2\omega_H) + \omega_M\alpha_k(1-\beta_k), \tag{A3}$$

and

$$T_k = S_k[s - (s+d)\beta_k]\alpha_k - 2\omega_M d\beta_k. \tag{A4}$$

The second-order dispersion parameter is

$$D_2 = \omega_M B_k\alpha_k + \frac{\omega_M}{(S_k^2 - 4\omega_M^2\beta_k)^{3/2}}[(S_k^2 - 4\omega_M^2\beta_k) \times (S_k B_k\alpha_k + \omega_M A_k^2\alpha_k^2 - 4\omega_M d^2\beta_k) - \omega_M T_k^2], \tag{A5}$$

where B_k is given by

$$B_k = s^2 - \beta_k(s+d)^2. \tag{A6}$$

The third-order dispersion parameter is given by

$$D_3 = -2\alpha_k\omega_M C_k - \frac{6\omega_M^3 T_k^3}{(S_k^2 - 4\omega_M^2\beta_k)^{5/2}} + \frac{6\omega_M^3 T_k(\alpha_k S_k B_k + \omega_M\alpha_k^2 A_k^2 - 2\omega_M d^2\beta_k}{(S_k^2 - 4\omega_M^2\beta_k)^{3/2}} - \frac{6\omega_M(\alpha_k S_k C_k + \omega_M\alpha_k^2 A_k B_k - 4\omega_M d^3\beta_k)}{(S_k^2 - 4\omega_M^2\beta_k)^{1/2}}, \tag{A7}$$

where C_k is given by

$$C_k = s^3 - \beta_k(s+d)^3. \tag{A8}$$

The nonlinear response parameter N is given by

$$N = -\frac{\omega_M}{4}\left\{\alpha_k(1-\beta_k) + \frac{S_k[2+\alpha_k(1-\beta_k)] - 4\omega_M\beta_k}{(S_k^2 - 4\omega_M^2\beta_k)^{1/2}}\right\}. \tag{A9}$$

The higher-order nonlinear response parameter Q is given by

$$Q = \frac{1}{2}\alpha_k\omega_m A_k - \frac{\omega_M^2 T_k\{S_k[2+\alpha_k(1-\beta_k)] - 4\omega_M^2\beta_k\}}{2[S_k^2 - 4\omega_M^2\beta_k]^{3/2}} + \frac{1}{2}\omega_m\frac{\alpha_k A_k\{S_k + \omega_M[2+\alpha_k(1-\beta_k)]\} - 4\omega_M d\beta_k}{2[S_k^2 - 4\omega_M^2\beta_k]^{1/2}}. \tag{A10}$$

[1] M. Chen, M. A. Tsankov, J. M. Nash, and C. E. Patton, Phys. Rev. B **49**, 12773 (1994).
[2] H. Xia, P. Kabos, C. E. Patton, and H. E. Ensle, Phys. Rev. B **55**, 15018 (1997).
[3] H. Xia, P. Kabos, R. A. Staudinger, C. E. Patton, and A. N. Slavin, Phys. Rev. B **58**, 2708 2715 (1998).
[4] H. Y. Zhang, P. Kabos, H. Xia, P. A. Kolodin, and C. E. Patton, Phys. Rev. B **61**, 522 (2000).
[5] B. A. Kalinikos, M. M. Scott, and C. E. Patton, Phys. Rev. Lett. **84**, 4697 (2000).
[6] M. M. Scott, B. A. Kalinikos, and C. E. Patton, Appl. Phys. Lett. **78**, 970 (2001).
[7] M. M. Scott, Y. K. Fetisov, V. T. Synogach, and C. E. Patton, J. Appl. Phys. **88**, 4232 (2000).
[8] H. Y. Zhang, P. Kabos, H. Xia, R. A. Staudinger, P. A. Kolodin, and C. E. Patton, J. Appl. Phys. **84**, 3776 (1998).
[9] C. E. Zaspel, P. Kabos, H. Xia, H. Y. Zhang, and C. E. Patton, J. Appl. Phys. **85**, 8307 (1999).
[10] V. I. Karpman, Phys. Lett. A **244**, 397 (1998).
[11] E. M. Gromov and V. I. Talanov, Chaos **10 (3)**, 551 (2000).
[12] C. E. Zaspel, Phys. Rev. Lett. **82**, 723 (1999).
[13] D. J. Frantzeskakis, K. Hizanidis, B. A. Malomed, and C. Polimilis, Phys. Lett. A **248**, 203 (1998).
[14] S. L. Palacios, A. Guinea, J. M. Fernandez-Diaz, and R. D. Crespo, Phys. Rev. E **60**, R45 (1999)

Downloaded 03 Jul 2003 to 129.82.31.230. Redistribution subject to AIP license or copyright, see http://ojps.aip.org/japo/japcr.jsp

[15] K. Yashiro and S. Ohkawa, IEEE Trans. Magn. **33**, 3439 (1997).
[16] A. D. Boardman, S. A. Nikitov, N. A. Waby, R. Putman, H. M. Mehta, and R. F. Wallis, Phys. Rev. B **57**, 10667 (1998).
[17] R. E. De Wames and T. Wolfram, J. Appl. Phys. **41**, 5243 (1970).
[18] W. L. Bongianni, J. Appl. Phys. **43**, 2541 (1972).
[19] A. D. Boardman and S. A. Nikitov, Sov. Phys. Solid State **31**, 281 (1989) [Sov. Phys. Solid State **31**, 1076 (1989)].
[20] S. A. Nikitov, S. Jun, R. Marcelli, and P. De Gasperis, J. Magn. Magn. Mater. **145**, L6 (1995).
[21] M. Uehara, K. Yashiro, and S. Ohkawa, Jpn. J. Appl. Phys. **38**, 61 (1999).
[22] A. S. Kindyak, Pis'ma Zh. Tekh. Fiz. **25**, 48 (1999) [Sov. Tech. Phys. Lett. **25**, 145 (1999)].
[23] G. P. Agrawal, Nonlinear Fiber Optics (Academic, San Diego, 1989).

Downloaded 03 Jul 2003 to 129.82.31.230. Redistribution subject to AIP license or copyright, see http://ojps.aip.org/japo/japcr.jsp